Texture-Based Modeling of Sheet Metal Forming and Springback

V. Schulze, A. Bertram, T. Böhlke, A. Krawietz

In this paper the application of a crystal plasticity model for body-centered cubic crystals in the simulation of a sheet metal forming process is discussed. The material model parameters are identified by a combination of a texture approximation procedure and a conventional parameter identification scheme. In the application of a cup drawing process the model shows an improvement of the strain and earing prediction as well as the qualitative springback results in comparison with a conventional phenomenological model.

1 Introduction

The simulation of sheet metal forming has become an important tool for the evaluation and optimization of forming processes. An important aspect to increase the accuracy of the simulations is the improvement of the material modeling. At present the material behavior is typically modeled by phenomenological material equations which do not take into account the evolving mechanical anisotropy due to a deformation induced texture development.

In the last years several phenomenological models have been suggested for the description of plastically anisotropic materials (see, e.g., Hill, 1948; Barlat and Lian, 1989; Barlat et al., 1991, 1997, 2003, 2005). Many of these models are based on linear transformations of the stress tensor and the application of the theory of isotropic tensor functions (Barlat et al., 2007). These phenomenological models usually assume that the anisotropy is initially known and generally constant during deformation. The missing micromechanical information is compensated by the fact that the computational effort of such an approach is fairly low. The first two models by Hill and Barlat are still standard for sheet metal forming simulations in an industrial environment due to the ease of the model identification and rather good correlations with practical measurements (Rohleder, 2002).

In contrast to these approaches, crystal plasticity models incorporate the microscopic structure of the material. This leads to the ability to predict the evolution of the macroscopic behavior due to changes on the micro-scale. This type of models has been studied intensively in the last decades. The early approaches by Sachs (1928) and Taylor (1938) introduced relatively coarse assumptions on the interaction of the grains and, consequently, on the homogenization of strains or stresses. The latter of these two models has been widely used (with some improvements (Bishop and Hill, 1951a,b)) due to a good correlation with experiments and the rather low computational costs of this model. In an effort to release the restrictive assumption of the Taylor-model, other models have been developed. One of the first attempts was to relax certain of the constraints for specific deformation modes, leading to the relaxed constraint models (Honneff and Mecking, 1978; van Houtte, 1981; Kocks and Canova, 1981), which have been refined further to enable the transition from the full to the relaxed constraint models (Tomé et al., 1984; van Houtte, 1988; Kocks and Necker, 1994). Another refinement for the crystal plasticity approach was the modeling of the interaction of the grains with the matrix having the effective properties of the material. This was achieved by the self consistent models (Eshelby, 1957; Kröner, 1961; Budiansky and Wu, 1962; Hill, 1965; Harren, 1991a,b). The latest development to improve the accuracy of this approach was the introduction of finite element simulations on the micro-scale (Harren and Asaro, 1989; Bronkhorst et al., 1992; Kalidindi and Anand, 1992; Dawson et al., 1994). The improvement of the model accuracy in these approaches has the price of a drastic increase in the computational effort, so that such micro-macro approaches are typically only used for virtual material tests.

A general way to reduce the degrees of freedom of a model based on crystal plasticity is the use of texture components (Wassermann, 1939; Bunge, 1993; Helming, 1996). A texture component is a crystal orientation for which the codf shows a (local) maximum in the elementary region. In its neighborhood, the codf is decreasing in an isotropic or anisotropic way. Raabe *et al.* (2002) and Raabe and Roters (2004) introduced the *texture component crystal plasticity method* defined by the simplification that each texture component is described by only one discrete crystal orientation. If a texture component is modeled in such a way, however, the mechanical anisotropy is

significantly overestimated. Raabe et al. suggested that in order to reduce this overestimation, the crystal orientations used in the finite element simulation should - from integration point to integration point - scatter around the mean orientations of the texture components in order to take into account the scattering of the crystallites around the ideal components. Such an approach has the disadvantage that the scattering is only taken into account on the average, i.e., if the whole sample is considered. Locally the mechanical anisotropy is still overestimated. Furthermore, an approach based on discrete random distributions induces a spurious mesh-dependence and does not generally ensure a reproducibility of the numerical results. Therefore, by Böhlke et al. (2006) it has been suggested to model the gray texture by an isotropic texture component given by an isotropic plasticity model and a corresponding volume fraction. Although this approach gives quite good results it has the inherent disadvantage that the evolution of the volume fraction of the isotropic texture component is rather difficult to model.

In addition to the pure phenomenological and the pure crystal plasticity models there have been studies to combine the low computational effort of the macro-model with the improved accuracy of the crystal plasticity models. In this course several ways have been pursued in order to generate analytical functions to approximate the yield surfaces derived by crystal plasticity models, using either the main components or the full ODF (Montheillet et al., 1985; Arminjon, 1985; Arminjon and Bacroix, 1990). Other models use a piecewise discretization for this approximation (Maudlin et al., 1996). The drawback of this approach is the assumption of full plasticity in the deformation of the crystals, resulting in problems to simulate loading and unloading situations.

The model used in this study is aimed to predict sheet metal forming operations and subsequent springback for body-centered cubic crystals for medium sized finite element models. For this aim we choose the Taylor assumption combined with a rate-independent pencil glide deformation model on the micro-scale as the crystal plasticity model. The hardening on the micro-scale is described by a phenomenological hardening law. Special emphasis is given to approximate the initial texture with a low number of crystals by a specific approximation schema. In order to reduce the anisotropy of the model, two different models for an isotropic background are examined and the results are compared with experimental measurements.

Notation. Throughout the text a direct tensor notation is preferred. The scalar product and the dyadic product are denoted by $\boldsymbol{A} \cdot \boldsymbol{B} = \mathrm{sp}(\boldsymbol{A}^\mathsf{T} \boldsymbol{B})$ and $\boldsymbol{A} \otimes \boldsymbol{B}$, respectively. A linear mapping of 2nd-order tensors is written as $\boldsymbol{A} = \mathbb{C}[\boldsymbol{B}]$. Traceless tensors (deviators) are designated by a prime, e.g., $\boldsymbol{A}'$. A superimposed bar indicates that the quantity corresponds to the macroscale.

2 Constitutive Equations

Elastic law. In the sequel we rely on the multiplicative decomposition of the deformation gradient $\boldsymbol{F}$ into an elastic part $\boldsymbol{F}_e$ and a plastic part $\boldsymbol{F}_p$, see e.g. (Lee, 1969; Mandel, 1974; Krawietz, 1986)

$$\boldsymbol{F} = \boldsymbol{F}_e \boldsymbol{F}_p. \tag{1}$$

The plastic deformation is assumed to be volume preserving such that $\boldsymbol{F}_p$ is unimodular, i.e. its determinant is equal to one. For rate-independent behavior, this decomposition can be derived from the concept of material isomorphisms (Bertram, 1999, 2005).

Since the elastic strains are assumed to be small, any linear relation between a generalized stress and a corresponding generalized strain measure can be used for the formulation of the elastic law. We apply the St. Venant-Kirchhoff law formulated in terms of quantities with respect to the undistorted configuration. Hence, the elastic law is given by

$$\boldsymbol{S}_e = \mathbb{C}[\boldsymbol{E}_e] \tag{2}$$

with $\boldsymbol{S}_e = \det(\boldsymbol{F}_e)\boldsymbol{F}_e^{-1}\boldsymbol{\sigma}\boldsymbol{F}_e^{-\mathsf{T}}$ the 2nd Piola-Kirchhoff stress tensor, $\boldsymbol{\sigma}$ the Cauchy stress tensor, $\boldsymbol{E}_e = (\boldsymbol{C}_e - \boldsymbol{I})/2$ Green's strain tensor and $\boldsymbol{C}_e = \boldsymbol{F}_e^\mathsf{T}\boldsymbol{F}_e$ the right (elastic) Cauchy-Green tensor.

Flow rule. The plastic flow is modeled by an evolution equation for the plastic part of the deformation gradient

$$\dot{\boldsymbol{F}}_p\boldsymbol{F}_p^{-1} = \sum_{\alpha \in \mathcal{A}}^{N} \dot{\gamma}_\alpha \, \boldsymbol{d}_\alpha \otimes \boldsymbol{n}_\alpha \tag{3}$$

with the slip rate $\dot{\gamma}_\alpha$, the slip direction $\boldsymbol{d}_\alpha$ and the slip plane normal $\boldsymbol{n}_\alpha$ of the slip system α. $\mathcal{A}$ denotes the set of active slip systems. N is the total number of slip systems.

The yield condition in each glide system is given by a scalar equation depending on the weighted shear stress τ_α and the critical resolved shear stress τ_α^C

$$\phi_\alpha(\tau_\alpha, \tau_\alpha^C) = |\tau_\alpha| - \tau_\alpha^C = 0. \tag{4}$$

The weighted shear stress τ_α is determined by the projection of the weighted Mandel stress tensor $\boldsymbol{Z}_e = \boldsymbol{C}_e \boldsymbol{S}_e / \varrho_0$ into the slip system

$$\tau_\alpha = \boldsymbol{Z}_e \cdot \boldsymbol{d}_\alpha \otimes \boldsymbol{n}_\alpha \tag{5}$$

with ϱ_0 being the mass density in the reference placement (Krawietz, 1999). If the yield condition and the loading condition are equally fulfilled, the consistency condition has to be satisfied for each active slip system

$$\dot{\phi}_\alpha = |\tau_\alpha|^\cdot - \dot{\tau}_\alpha^C = 0. \tag{6}$$

Pencil glide. Body-centered cubic crystals (bcc) have 48 primary glide systems. For a rate-independent material law, an admissible combination of the glide systems has to be determined that satisfies the yield condition (4) and the consistency condition (6). A systematic testing sequence would be very time consuming. For the case of bcc crystals, this cumbersome procedure can be reduced by using the pencil glide model. Since the possible glide planes are very close to each other, in this model all planes are possible glide planes if they have a normal being orthogonal to the glide direction. This reduces the number of glide systems to four.

In the context of pencil glide for given slip directions $\boldsymbol{d}_\alpha$ corresponding to the lattice directions $\langle 111 \rangle$, the slip plane normals $\boldsymbol{n}_\alpha$ are to be determined. The slip plane normal $\boldsymbol{n}_\alpha$ which is normalized and perpendicular to the corresponding slip direction $\boldsymbol{d}_\alpha$ is extremizing the shear stress τ_α given by (5). Hence the $\boldsymbol{n}_\alpha$ can be determined by the Lagrange multiplier method with the Lagrange function

$$\mathcal{L} = \boldsymbol{Z}_e \cdot \boldsymbol{d}_\alpha \otimes \boldsymbol{n}_\alpha - \lambda \, \boldsymbol{d}_\alpha \cdot \boldsymbol{n}_\alpha - \frac{\mu}{2} \left(\boldsymbol{n}_\alpha \cdot \boldsymbol{n}_\alpha - 1 \right) \tag{7}$$

containing the Lagrange multipliers λ and μ. The derivative with respect to $\boldsymbol{n}_\alpha$ yields

$$\frac{\partial \mathcal{L}}{\partial \boldsymbol{n}_\alpha} = \boldsymbol{Z}_e^\mathsf{T} \boldsymbol{d}_\alpha - \lambda \boldsymbol{d}_\alpha - \mu \boldsymbol{n}_\alpha = \boldsymbol{0} \tag{8}$$

or equivalently

$$\mu \boldsymbol{n}_\alpha = \boldsymbol{Z}_e^\mathsf{T} \boldsymbol{d}_\alpha - \lambda \boldsymbol{d}_\alpha. \tag{9}$$

The Lagrange multipliers λ and μ follow from $\boldsymbol{n}_\alpha \cdot \boldsymbol{d}_\alpha = 0$ and $\boldsymbol{n}_\alpha \cdot \boldsymbol{n}_\alpha = 1$, respectively. The first condition implies

$$\lambda = \boldsymbol{d}_\alpha \cdot (\boldsymbol{Z}_e \boldsymbol{d}_\alpha). \tag{10}$$

Hence $\boldsymbol{n}_\alpha$ is

$$\boldsymbol{n}_\alpha = \frac{1}{\mu} \boldsymbol{s}_\alpha, \qquad \boldsymbol{s}_\alpha = (\boldsymbol{I} - \boldsymbol{d}_\alpha \otimes \boldsymbol{d}_\alpha) \boldsymbol{Z}_e^\mathsf{T} \boldsymbol{d}_\alpha, \qquad \mu = \|\boldsymbol{s}_\alpha\| \tag{11}$$

For a given stress state $\boldsymbol{Z}_e$, eq. (11) determines a shear vector for each slip direction $\boldsymbol{d}_\alpha$. Since the vector $\boldsymbol{s}_\alpha$ is orthogonal to the glide direction $\boldsymbol{d}_\alpha$, one derives the result

$$\tau_\alpha = \boldsymbol{s}_\alpha \cdot \boldsymbol{n}_\alpha = \|\boldsymbol{s}_\alpha\| = \mu. \tag{12}$$

Hardening rule. The hardening is modeled by a phenomenological approach based on an accumulated slip in each slip system. We assume that the critical weighted shear stress τ_α^C depends on a hardening parameter ξ_α defined by

$$\dot{\xi}_\alpha = (1 - q) \dot{\gamma}_\alpha + q \sum_\beta \dot{\gamma}_\beta, \tag{13}$$

where q is the ratio of self and latent hardening. The hardening can be modeled for example by the ansatz of Swift

$$\tau_\alpha^C = A_1 \left(1 + A_2 \xi_\alpha \right)^n. \tag{14}$$

In order to model a hardening behavior with a pronounced yield limit, the following ansatz is presently preferred

$$\tau_\alpha^C = A_1 \left(1 + A_2 \left(\sqrt{A_3^2 + \xi_\alpha^2} - A_3 \right) \right)^n, \tag{15}$$

137

where the A_i and n are fitting parameters for the yield curve. A_3 allows for a modeling of a pronounced yield strength. For $A_3 = 0$ the Swift ansatz is obtained.

Homogenization of the constitutive behavior. The aim is to perform a finite element simulation on the macroscale and to simultaneously take into account the crystallographic texture on the grain scale. The relation between the macroscopic and mesoscopic stress and strain measures can be determined, e.g., by Taylor type models (Taylor, 1938; Asaro, 1985; Mathur and Dawson, 1989). The Taylor model assumes a homogeneous deformation field through the microstructure of polycrystals. Therefore, it satisfies the strain compatibility, but not the stress equilibrium at the grain boundaries. The Taylor model gives reasonable qualitative approximations of the crystallographic texture evolution in many single-phase cubic materials, but it is known to significantly overestimate the stresses and the texture sharpness. Due to the general shortcomings of the Taylor model, different approaches have been discussed in the literature in order to improve the modeling of the texture evolution. The most simple one is based on a relaxation of certain constraints of the deformation field (RC Taylor models). A typical example is the LAMEL model by van Houtte (1982), which has been developed to predict rolling textures. Roughly speaking, the model takes a stack of two grains, which is compressed, and permits an inhomogeneous deformation. This allows to satisfy the stress equilibrium for the shear stresses within the flattening plane. The disadvantage of the model is that it is only applicable for one specific deformation mode. The GIA model (Crumbach et al., 2001) is applicable for general deformation paths. Due to the more complex modeling of the grain interaction the premises for the texture prediction are better than for the LAMEL model. For a comparison see van Houtte et al. (2002, 2006). Another quite successful approach is given by the class of self-consistent approximations of the local deformation behavior (e.g., Molinari et al., 1987), which satisfy the strain compatibility and the stress equilibrium in an averaged sense. A purely numerical approach for a detailed description of the microstructure is given by the representative volume element technique based on finite elements and crystal plasticity (Bronkhorst et al., 1992), sometimes referred to as CPFEM (crystal plasticity finite element model). For a review of the aforementioned methods with special emphasis to sheet metal forming see the excellent review by Dawson et al. (2003). Since the computational effort of homogenization schemes based on non-homogeneous strain fields is significantly higher than that of the Taylor model, and since we aim to describe a real metal forming operation, Taylor's assumption of a homogeneous deformation field is applied here, i.e.

$$\boldsymbol{F} = \bar{\boldsymbol{F}}. \tag{16}$$

A justification of this coarse assumption will only be possible based on the results discussed below. The effective Cauchy stress is calculated as the volume average of the crystal stresses with respect to the current volume. For polycrystals consisting of M grains with homogeneous orientation this yields

$$\bar{\boldsymbol{\sigma}} = \frac{1}{v} \int_v \boldsymbol{\sigma} \, \mathrm{d}v = \sum_{\beta=1}^{M} c_\beta \, \boldsymbol{\sigma}_\beta, \tag{17}$$

where c_β is the volume fraction of grain β. This is equivalent to computing the effective 1st Piola-Kirchhoff stress tensor by volume averaging with respect to the initial placement.

Modeling of the gray texture. From the numerical point of view, large-scale computations based on the Taylor model are very time-intensive and storage-consuming if the crystallographic texture is approximated by several hundred discrete crystals. In the present work we use two different approaches in order to model the gray texture. In the first approach, a small group of crystals having a perfect elastic isotropy in the sense of the bounds by Voigt and Reuss (Bertram et al., 2000; Böhlke, 2001; Böhlke and Bertram, 2001) is used in the initial setup. In the second approach an isotropic von Mises plasticity model with fictitious volume fraction is used (hybrid model). In this case the elastic law is given by eq. (2) with $\mathbb{C}$ being isotropic. The evolution of $\boldsymbol{F}_p$ is modeled by a normality rule

$$\dot{\boldsymbol{F}}_p \boldsymbol{F}_p^{-1} = \dot{\gamma} \boldsymbol{N} \tag{18}$$

with

$$\boldsymbol{N} = \frac{\boldsymbol{Z}_e'}{\|\boldsymbol{Z}_e'\|} \approx \frac{\boldsymbol{S}_e'}{\|\boldsymbol{S}_e'\|}. \tag{19}$$

The yield condition is

$$\|\boldsymbol{S}_e'\| - \sqrt{\tfrac{2}{3}} \sigma_F = 0. \tag{20}$$

3 Identification of Texture and Material Parameters

Texture measurement. The material used for the following examples are typical ferritic deep drawing steel grades. The first material considered is DX53, a mild deep drawing grade, while the second material is the high strength low alloyed steel H340LAD. For the identification of a crystal plasticity model, the initial texture of the material has to be measured and approximated by the initial orientation of the crystals and their respective volume fraction. In a second step the parameters for the elastic and plastic constants are determined similar to a conventional phenomenological model. The crystallographic texture of a material can be measured by the scatter of a high energy beam, such as x-rays, electron beams, or neutron beams on the crystal lattice (Bunge, 1993; Schumann et al., 1991). In addition, different preparation methods can be used in order to determine a representative texture of a material with a texture gradient (Bunge and Welch, 1983; Welch, 1980).

Since the model should be used for an industrial application, and due to the fact that only the orientation distribution function is of interest for the following texture approximation, the steel sheets are measured by conventional x-rays. A surface measurement is sufficient for the characterization of the material, because the texture thickness gradients in the thin sheets (1 mm) under consideration are negligible.

Approximation of the initial texture. The approximation of the initial texture is of high importance not only for the accuracy of the model but also for the computational effort in the consecutive finite element simulation. Consequently, this approximation has been the field of special studies by several authors (Toth and Van Houtte, 1992; Kocks et al., 1991; Helming, 1996; Delannay et al., 2000; Cho et al., 2004; Tarasiuk et al., 2004). Since these methods either need special skills of the operator, are designed for specific textures, or lead to approximations with a large number of crystals, a different approximation scheme is used in this work. This method is based on a mixed integer quadratic approximation scheme using sharp components with a joint scatter width to approximate a given texture (Böhlke et al., 2006). The advantage of this method is that it can be applied to arbitrary crystal and texture classes, the existence of an error bound for the approximation, and the user-independence of the approximation results. With this approximation the initial orientation of the crystals as well as their respective volume fraction can be determined in one optimization procedure.

Identification of the material parameters. Since the material model should be applied in an industrial environment, the identification of the model parameters has to be performed using only a small set of measurements. Due to this condition, simple tension tests in three directions with respect to the rolling direction have been used to characterize the material.

For the determination of the elastic material parameters, the Young's modulus has been measured at $0°$, $45°$ and $90°$ with respect to the rolling direction, using tension test specimens of type 2 according to DIN-EN 10002-1. For the determination of the Young's modulus, the stress has been increased at a stress rate of 20 MPa/s. The same approach has been used to determine the yield curves and the r-value in the respective directions. For these measurements, the tests have been performed at a global strain rate of 0.4%/s. The r-value describes the ratio of the strains in the width to the thickness direction

$$r = \frac{\ln(b/b_0)}{\ln(t/t_0)} = \frac{\ln(b/b_0)}{\ln((b_0 l_0)/(bl))}, \tag{21}$$

where b is the width, t is the thickness and l is the length of the specimen. The index 0 denotes the initial value of the respective parameter. The results of these tension tests are given in Table 1.

Material	Angle wrt. RD	E in GPa	$R_{p0,2}(*R_{eH})$ in MPa	r value
DX53D+Z	0°	179	159	2,02
DX53D+Z	45°	196	166	1,54
DX53D+Z	90°	190	164	2,39
H340LAD	0°	201	381*	0.78
H340LAD	45°	203	379	1,07
H340LAD	90°	210	401	1,10

Table 1: Measured material parameters

For the approximation of the gray texture two approaches are used. The first approach (ISO12) is the use of a small group of 12 crystals having initially a perfect elastic anisotropy (Bertram et al., 2000; Böhlke and Bertram, 2001). While the elastic behaviour of cubic crystals is determined by three texture coefficients (Bunge, 1993), the determination of the plastic parameters needs further coefficients. Consequently, the plastic behaviour of this group is not perfectly isotropic.

A macroscopic von Mises model on the micro scale is used in the second approach to approximate a single isotropic crystal. This model has two advantages: Firstly, it is perfectly isotropic, with respect to both the elastic and plastic behaviour. Secondly, the computational effort is dramatically reduced compared with the crystal group. For simplicty, we assumed a constant isotropic volume fraction during the deformation process.

The approximation of the isotropic volume fraction is performed by a least square fit of the distribution of the r-values. A good initial estimation for this volume fraction is given by the approximation procedure for the initial texture. A modification of the volume fraction of the gray texture has only influence on the height of the r-values but not on the distribution of the minimal and the maximal magnitudes, which are determined by the orientation and respective weight of the crystals.

Using the measurement of the Young's modulus in the three directions and taking into account the material and crystal symmetry, the missing elastic parameters can be determined. For that purpose, we consider the harmonic decomposition of the stiffness tensor $\mathbb{C}$ of one individual cubic crystal (Böhlke, 2001)

$$\mathbb{C} = 3K\mathbb{P}_1 + 2G\mathbb{P}_2 + \mathbb{H}', \tag{22}$$

where

$$\mathbb{P}_1 = \frac{1}{3}\boldsymbol{I} \otimes \boldsymbol{I}, \qquad \mathbb{P}_2 = \mathbb{I}^S - \mathbb{P}_1 \tag{23}$$

are the two isotropic projectors governing isotropic linear elastic behavior and

$$\mathbb{H}' = \frac{1}{5}\left(\lambda_3 - \lambda_2\right)\left(2\mathbb{I}^S + \mathbf{1} \otimes \mathbf{1} - 5\mathbb{D}\right) \tag{24}$$

with

$$\mathbb{D} = \sum_{\alpha=1}^{3} \boldsymbol{g}_\alpha \otimes \boldsymbol{g}_\alpha \otimes \boldsymbol{g}_\alpha \otimes \boldsymbol{g}_\alpha \tag{25}$$

is the harmonic part of the decomposition. The bulk modulus K and the shear modulus G of the isotropic part can be determined by the eigenvalues λ_i of the stiffness tensor of the single crystal: $3K = \lambda_1, 2G = 2\lambda_2/5 + 3\lambda_3/5$.

$\boldsymbol{I}$ is the 2nd-order identity tensor. $\mathbb{I}^S$ is the 4th-order identity tensor on symmetric 2nd-order tensors. The purely anisotropic part $\mathbb{D}$ of the decomposition depends on the lattice vectors $\boldsymbol{g}_\alpha$. Since the measured elasticity parameters represent effective material properties and the modeling is based on the Taylor assumption, we compute the Voigt average of the elasticity tensor in the context of small strains. One obtains

$$\mathbb{C}^{VC} = 3K\mathbb{P}_1 + 2G\mathbb{P}_2 + \mathbb{H}'^V \tag{26}$$

with

$$\mathbb{H}' = \frac{1}{5}\left(\lambda_3 - \lambda_2\right)\left(2\mathbb{I}^S + \boldsymbol{I} \otimes \mathbf{1} - 5\mathbb{D}^V\right), \qquad \mathbb{D}^V = \sum_{\beta=1}^{M} c_\beta \, \mathbb{D}(\boldsymbol{g}_\alpha^\beta). \tag{27}$$

In the case of the approximation of the gray texture by the von Mises model, the corresponding stiffness tensor is given by

$$\mathbb{C}^{MI} = 3K\mathbb{P}_1 + 2G\mathbb{P}_2. \tag{28}$$

The total elasticity tensor is then

$$\mathbb{C}^V = c_{VC}\,\mathbb{C}^{VC} + c_{MI}\,\mathbb{C}^{MI}, \tag{29}$$

where c_{MI} is the volume fraction of the isotropic background. Using this approach, the von Mises model is consistently identified, and the number of elastic parameters to be identified is kept constant. Due to the nonlinearity of the resulting equations and the accuracy of the texture measurement, the approximation is performed by a least square optimization procedure using a simplex algorithm with bounds for the allowable values of the elastic parameters.

The approximation of the plastic response of the crystals is done by the adjustment of four parameters according to a hardening law (15). Furthermore, the initial hardening parameters $\zeta_{0,i}$ of the crystals have to be determined. For this approximation, the three yield curve measurements are used. The calibration is performed in the range of a homogeneous deformation of the sample specimen. For the approximation, the tension test is simulated and the parameters are calibrated by a sequential approximation scheme. In the case of the hybrid model, the isotropic part is first adjusted to the average yield curve of all three directions

$$\sigma_{iso}\left(\varphi\right) = \frac{\sigma_0\left(\varphi\right) + 2\sigma_{45}\left(\varphi\right) + \sigma_{90}\left(\varphi\right)}{4}. \tag{30}$$

After this approximation, the plastic parameters of the crystals are determined. The results of this procedure are given in Table 2 and Table 3.

	E in GPa	G in GPa	ν	q	A_1 GPa	A_2	A_3	n	ξ_0	v_{iso}
A16I12	110.30	94.90	0.3542	1.4	0.0278	404.400	0.0	0.281	0.0039228	0.72
A48I12	113.27	94.49	0.3474	1.4	0.0294	412.590	0.0	0.269	0.0330004	0.71
A80I12	113.20	94.47	0.3476	1.4	0.0294	413.365	0.0	0.269	0.0330349	0.71
A16M	114.88	94.99	0.3302	1.4	0.0299	410.090	0.0	0.275	0.0330500	0.56
A32M	114.35	94.82	0.3320	1.4	0.0292	409.970	0.0	0.270	0.0330500	0.54
A48M	111.60	95.00	0.3415	1.4	0.0271	400.147	0.0	0.278	0.0326575	0.54
A64M	113.97	94.71	0.3304	1.4	0.0291	414.920	0.0	0.270	0.0330500	0.52
A80M	114.30	94.81	0.3307	1.4	0.0292	409.960	0.0	0.270	0.0330400	0.52
A96M	113.75	94.63	0.3334	1.4	0.0292	409.940	0.0	0.270	0.0330400	0.50

Table 2: Material parameters of DX53 D+Z

	E in GPa	G in GPa	ν	q	A_1 GPa	A_2	A_3	n	ξ_0	v_{iso}
B16I12	115.58	116.16	0.3146	1.4	0.1414	1712.5	1.504	0.07	2.636E-04	0.97
B48I12	115.54	95.18	0.4404	1.4	0.1410	1712.5	1.506	0.07	3.619E-04	0.94
B80I12	115.54	101.79	0.3952	1.4	0.1410	1712.5	1.506	0.07	4.609E-04	0.92
B16M	145.60	95.25	0.3589	1.4	0.1319	1688.0	0.800	0.07	2.600E-04	0.92
B32M	148.50	95.20	0.3477	1.4	0.1319	1687.8	0.803	0.07	2.589E-04	0.89
B48M	143.05	95.20	0.3630	1.4	0.1303	1697.8	0.803	0.07	2.49E-04	0.85
B64M	145.25	95.20	0.3413	1.4	0.1317	1697.0	0.800	0.07	2.589E-04	0.83
B80M	145.15	95.20	0.3571	1.4	0.1319	1687.7	0.803	0.07	2.598E-04	0.83
B96M	146.71	95.20	0.3509	1.4	0.1310	1691.6	0.724	0.07	2.650E-04	0.79

Table 3: Material parameters of H340LAD

4 Application to Deep Drawing and Springback

Previous work. The earing of a cylindrical cup drawn from a circular blank is a result of the anisotropy of the material and therefore a measure for the accuracy of the material model. One result of this study is the fact that Hill's quadratic yield criterion (Hill, 1948) is unable to predict more than 4 ears. While this is sufficient for typical steels, it is insufficient for aluminum, which can form up to 8 ears. In order to be able to predict this behavior, more sophisticated models have been derived and tested. Becker (1993); Yoon and Hong (2006) have used the cup drawing procedure to test yield surfaces of Barlat et al. (2003, 2005) for aluminum. Also the crystal plasticity based models have been evaluated using this method: Hu et al. (1998) evaluated the influence of the friction, the blank holder force and the element type on the earing with a forth order plastic strain rate potential derived from the texture of the material. The combination of a plastic potential with a microstructural based hardening model has been used by Li et al. (2003) to simulate the cup drawing of an IF-steel. Engler and Hirsch (2007) studied the influence of different textures on the earing profile both experimentally and by the simulation based on a visco-plastic self-consistent model. Recent studies used this method to numerically determine the influence of certain texture components in steel by a texture based crystal plasticity model (Raabe et al., 2005) and the influence of texture gradients in on the accuracy of such models (Tikhovskiy et al., 2008).

The springback behavior is a measure for the ability of a model to predict the internal stresses in the material correctly. The simulation with finite elements started with simple processes, such as plane bending processes (Makinouchi, 1984; Mattiasson et al., 1995) or hat-profiles (Wagoner and He, 1996). More complex and realistic shapes have been used in the following years to study the influence of different parameters (i.e. the number of integration points in thickness direction, influence of friction, element size, contact formulation), such as the studies by Hu et al. (1998); Valente and Traversa (1999); Wagoner and He (1996); Xu et al. (2004). In the work by Rohleder (2002) a comparison of commercial forming codes has been performed and suggestions for simulation parameters are derived from simple drawing processes (s-rail), small process chains (deep drawing and cutting) up to complex deep drawing operations with several forming steps of a typical automotive part. In the paper by Yoshida and Uemori (2003) it was shown that the incorporation of the deformation induced anisotropy improves the accuracy of the springback prediction of a u-shaped structure. The work by Andersson (2005) evaluated the springback behavior of different steels on a front side member of a car, using the Barlat 1989 model. This study reveals the influence of the modeling of the draw-beads on the simulation results for complex forming operations. The Barlat 1989 model was also used as one yield criterion in the study by Dongjuan et al. (2006) which compared the standard isotropic hardening with a nonlinear kinematic hardening law as well as other yield criteria (Hill 1948) in a 2D example. The study by Wagoner (2007) was focused on the question of the number of integration points needed for a certain accuracy of the springback results. Using the information of these earlier work, the number of integration points and the contact handling have been chosen for this study.

Experimental work. For the verification of the material model, a deep drawing test of a circular cup is used. Subsequent to the deep drawing, the cups are cut into slices and these rings are opened so that the springback of the part can be evaluated (Rohleder, 2002). The cup has a diameter of 150 mm and a drawing depth of 91.8 mm. The die radius is 6.5 mm while the punch radius is 8.5 mm. Figure 1 shows the tool in the experimental setup. During the drawing process, the blank holder force is set to 500 kN and the punch velocity to 30 mm/s. In order to reach the necessary drawing depth, a lubricant is used.

Figure 1: Cup drawing tool setup

For the model verification, the strain field and the cup geometry, and in particular the shape of the rim are measured by optical means.

Figure 2: Springback experiment: cup, rings, open rings

For the springback evaluation, a group of cups is first sliced into rings and then opened by wire-EDM. The diameter of the rings prior and after the opening is determined by an optical measurement. The change of the ring diameter is a measure for the internal stresses in the part after the forming process (Rohleder, 2002). The three steps of the springback evaluation are shown in Fig. 2. It can be seen that the amount of the diameter change depends on the position of the ring within the cup. The diameter of the rings has been calculated by a least square approximation of an ideal circle to the normal projection of the measurement points onto the cutting plane.

Simulation of a deep drawing process. For the simulation of the deep drawing process, the CAD-geometry of the tools is meshed with shell elements on the contact surfaces. The shells belonging to the tools are rigid bodies that are only used for the contact determination. For this reason it is necessary to avoid angles higher than 7.5° between the normals of neighboring shell elements. The blank is modeled by deformable shell elements. The elements used here are underintegrated Belytschko-Lin-Tsay (Hallquist, 1998) elements, which are routinely used in industrial simulations.

The crystal plasticity model is to be compared with a standard material model used for deep drawing simulations in industry. This model is a three parameter Barlat 1989 model (Barlat and Lian, 1989), which has been implemented in LS-Dyna (Hallquist, 1998). This model can be used with an exponent $m = 2$ resulting in a von Mises-Hill type yield behavior with an additional shear-stress influence. As an alternative for bcc materials, the exponent is to be set to $m = 6$ (Hallquist, 1998). This model is able to take into account the in plane anisotropy by using the r-values at $0°$, $45°$ and $90°$ with respect to the rolling direction. For the yield curve, the average yield curve in the rolling direction is used with a tangent linear extrapolation up to a true strain $\varphi = 1$.

Due to the material and process symmetry it is necessary to simulate at least one half of the cup for the deep drawing process (Fig. 3), since the springback process has only one symmetry plane. For the reduction of the computational costs, the simulation has been performed by an adaptive mesh refinement. Furthermore, the tool velocity is increased. The tool speed is increased continuously with a sinusoidal function to the maximum and reduced in the same way.

The contacts between the tool and the blank are taken into account with normal and tangential nodal forces. The stiffness of the tools is modeled by a penalty contact law, since the model is used for the springback evaluation. The friction between the interacting surfaces is approximated by a Coulomb law with static friction coefficients for each interface.

Simulation of the springback. For the springback simulation it is of high importance to approximate the stress distribution in the thickness direction of the shell. This is done by the use of 7 or 9 integrations points in the thickness direction during the deep drawing simulation and the subsequent springback calculation. These values are chosen according to the results of other studies by (Rohleder, 2002). After the initial forming operation, the
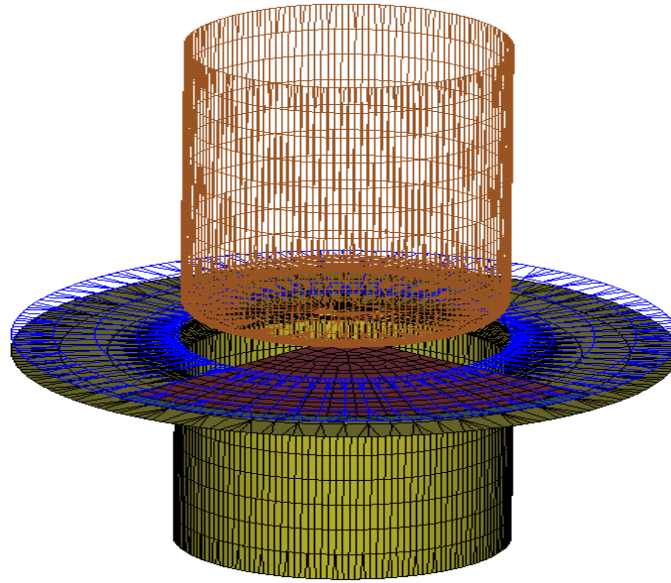
Figure 3: FEM model for the deep drawing simulation

model is interactively cut into the rings using Dynaform. For the crystal plasticity model, the user variables are mapped after the geometrical cutting procedure to the new mesh in an initialization run.

In order to simulate the cutting, the symmetry boundary conditions on one side of the ring are released, while on the other side all rigid body motions are permitted for the use of an implicit integration scheme. The position of the nodes at the end of the deformation is then projected onto the cutting plane and approximated by an ideal circle to determine the diameter change in the same way as the experimental values are determined.

Results. For the simulation of the deep drawing process, different configurations of the crystals are used. The abbreviations are as follows. The letter at the beginning of the name characterizes the material, A is DX53D+Z and B is H340LAD. The following number characterizes the amount of crystals used to approximate the anisotropic part of the initial texture. In case of the application of the ISO12-configuration for the approximation of the isotropic background (I), an additional group of 12 crystals is used, therefore the overall number of crystals in this case is the sum of both groups. In case of the hybrid model (M), only the 'isotropic background' is added to the group. The last digit characterizes the number of integration points in thickness direction. For reference, the Barlat 1989 model is characterized similarly. The first number is equal to the exponent, and the "B" stands for the Barlat 1989 model.

For the friction coefficient, a value of $\mu = 0,075$ for DX53D+Z and $\mu = 0,070$ for H340LAD has been measured and used for the simulation. The penalty parameter is equal to the suggested value for LS-Dyna (Hallquist, 1998). The results of strain distributions for DX53D+Z are given in Fig. 4 - 7. The strain cuts show a distinct increase in the accuracy of the prediction of the major and minor strains compared with the reference model.

Considering the prediction of the earing, the result is improved by the application of the crystal plasticity model in combination with the von Mises model for the background. Only the model with 16 crystals is unable to reproduce the shape of the earing after the deformation (Fig. 8). For the models with 32 or more crystals, the result is in good agreement with the measurements. The mean error of the flange draw-in is reduced from more than 3.3 mm in the reference model to less than 1.6 mm with the crystal models. The earing height predicted by the Barlat models is in the range of more than 10 mm while it is less than 4 mm with the hybrid models with more than 32 crystals, and, therefore, within the range of the measurements (3,6 mm ± 0,7 mm).

The application of the ISO12 model for the isotropic background results in quite different findings. With an increasing number of crystals, the shape of the earing deviates more from the measurements (Fig. 9). The reason for this behavior is the weighting factor used for the crystals in this group. The overall isotropic volume fraction is decreasing with an increasing number of crystals. However, at the same time the individual weight of these crystals is reduced. Therefore, the relative weight of the ISO12-group is increasing. Consequently, the earing is dominated

by the shape generated by these crystals.

The results of the springback evaluation are given in Fig. 10, 11 and Table 4. The measurements show a closing of the lowest ring (4) after the opening cut. The maximum diameter is observed at the second highest ring (2), while the highest ring has a slightly smaller diameter.

Distance from bottom	15 mm	35 mm	55 mm	75 mm
	r in mm	r in mm	r in mm	r in mm
Meas.	73,4	86,3	88,4	87,7
A2B7	76,4	96,5	106,4	110,2
A2B9	76,3	96,1	99,1	107,8
A6B7	74,4	89,0	93,6	100,1
A6B9	73,8	89,3	93,4	98,1
A16I7	75,0	89,8	90,9	93,9
A16M7	74,7	92,0	95,0	95,9
A16M9	74,7	88,8	92,5	95,0
A32M7	74,1	90,7	92,9	95,0
A48I7	75,0	89,8	91,0	85,4
A48M7	74,1	90,9	92,6	94,6
A48M9	74,2	89,1	91,3	93,5
A64M7	74,3	91,5	94,2	95,6
A80I7	75,0	89,8	90,7	84,6
A80M7	74,1	91,3	93,4	95,6
A80M9	74,3	91,5	93,5	94,9
A96M7	74,3	91,2	93,3	95,6

Table 4: Results of the springback simulation with DX53D+Z

The crystal models with 7 integration points in thickness direction give a good prediction of the springback. The closing of ring 4 is predicted well by all crystal plasticity models, while the Barlat 1989 model with the exponent of $m = 2$ fails to predict this behavior. In contrast to the measurements, all simulations predict the maximum diameter at the highest ring (1), however, the differences between ring 1 and 2 are small with the crystal plasticity model in combination with the von Mises model. The maximal error of the crystal models is also smaller than the one of the Barlat 1989 model.
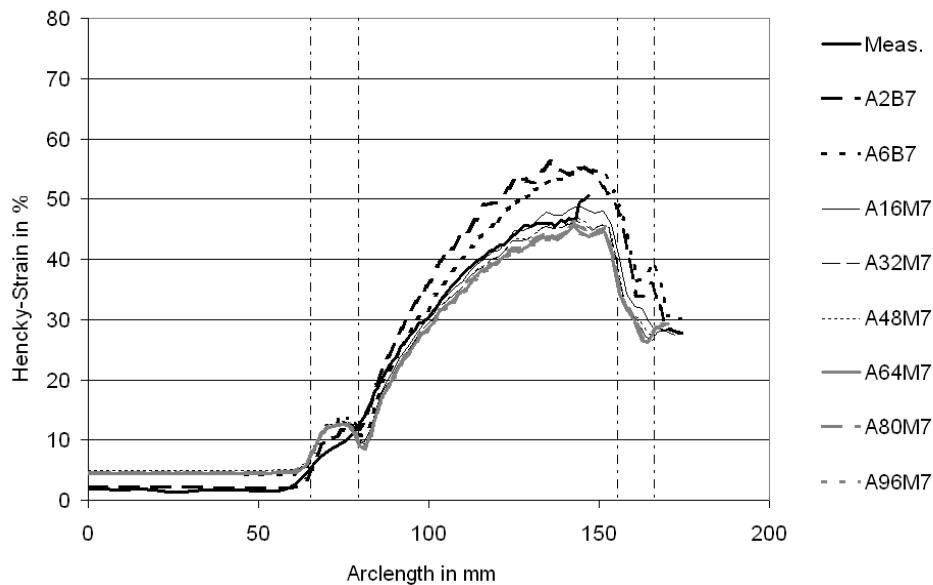
Figure 4: Major strain in rolling direction (isotropic von Mises component, DX53)
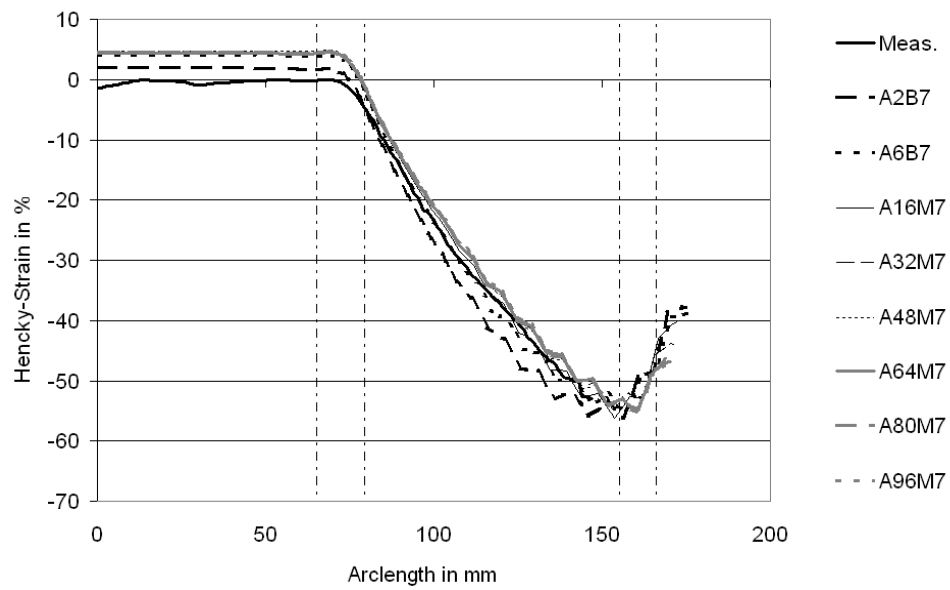
Figure 5: Minor strain in rolling direction (isotropic von Mises component, DX53)
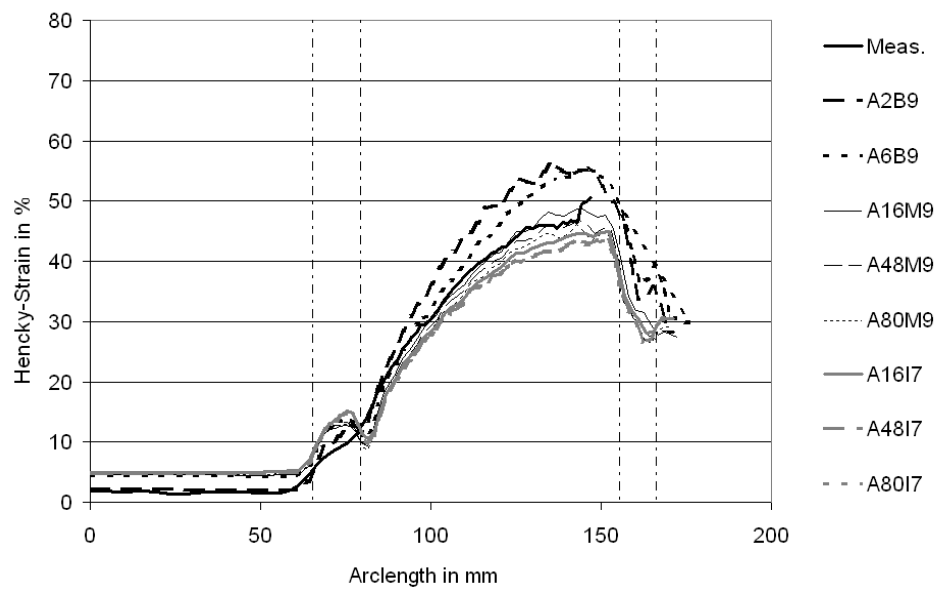

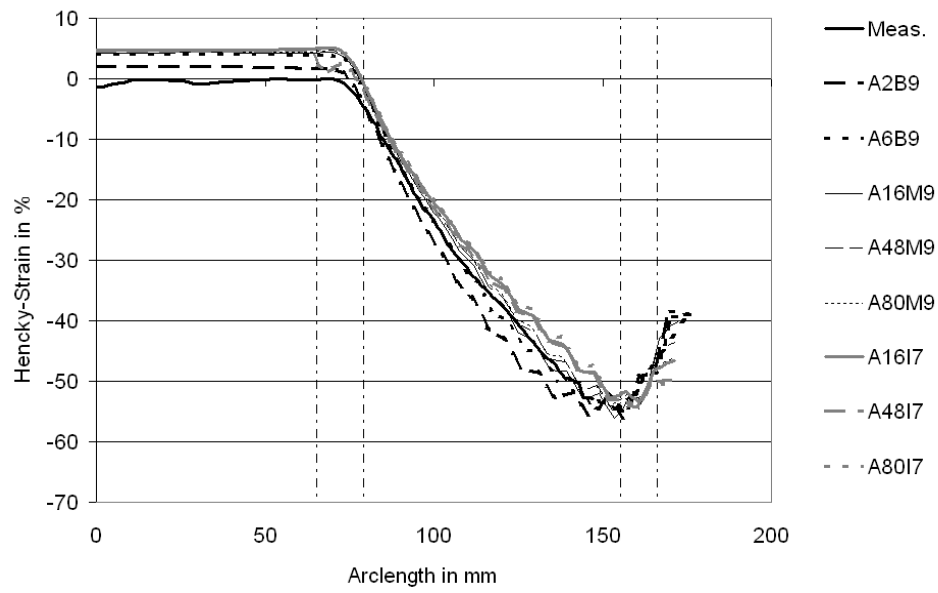Figure 6: Major strain in rolling direction (ISO12 background, DX53)

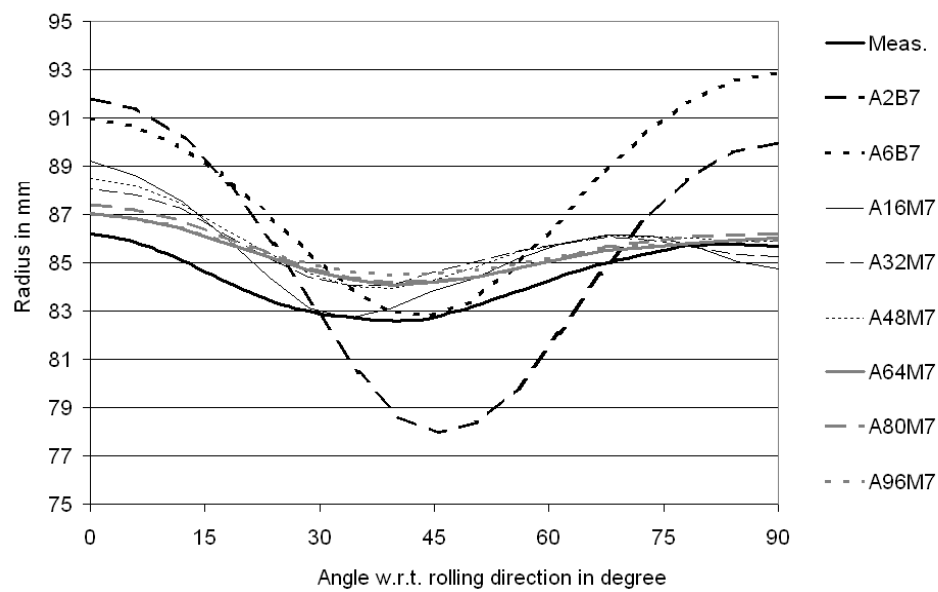Figure 7: Minor strain in rolling direction (ISO12 background, DX53)

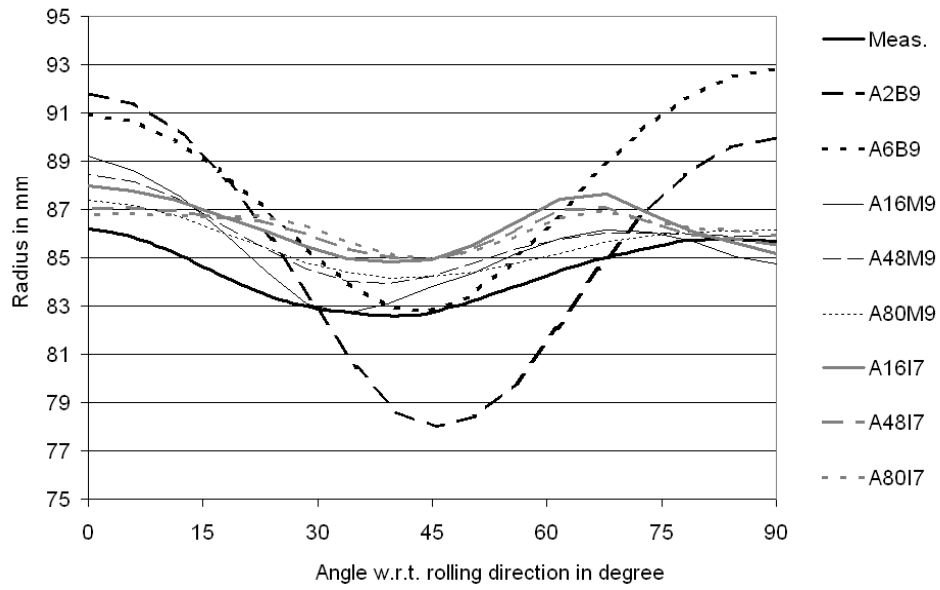Figure 8: Earing profile for models with isotropic von Mises component (DX53)

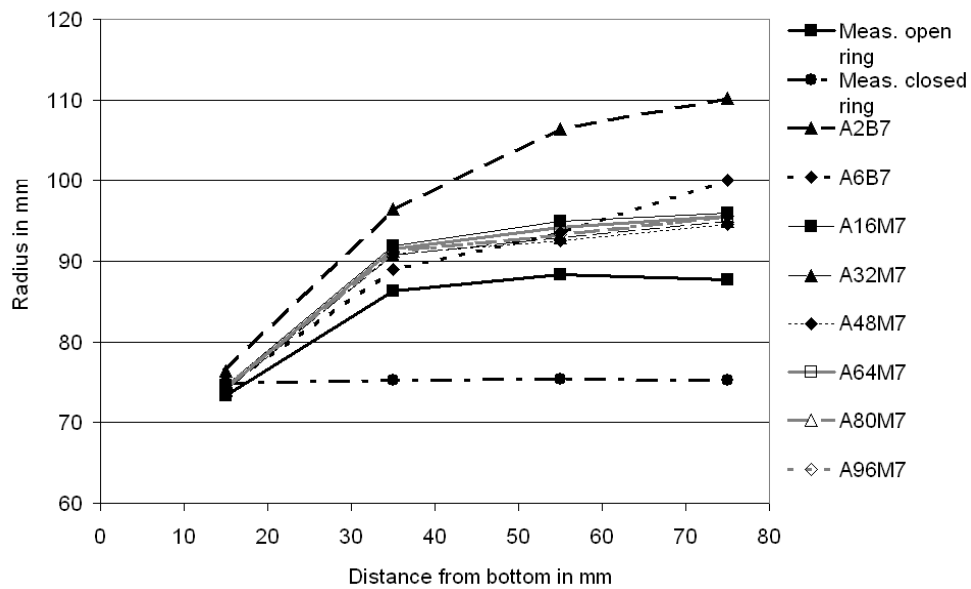Figure 9: Earing profile for models with ISO12 background and isotropic von Mises component (DX53)

Figure 10: Springback results of DX53D+Z: Distribution of the ring radii Barlat 1989 model (7 IP), crystal model isotropic von Mises component (7 IP)
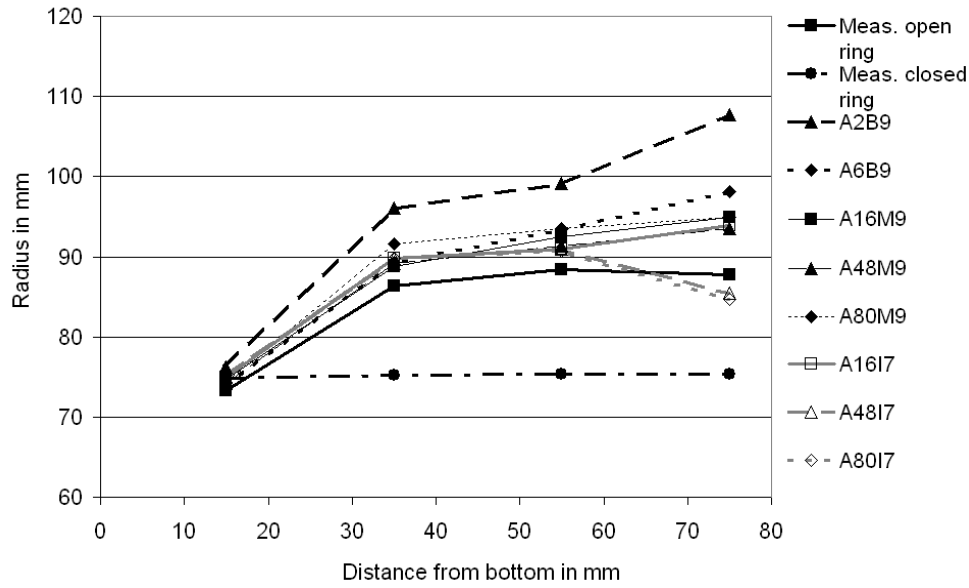
Figure 11: Springback results of DX53D+Z: Distribution of the ring radii, Barlat 1989 model (9 IP), crystal model with von Mises background (9 IP), crystal model with ISO12 background (7 IP)

The increase of the number of integration points in thickness direction increases the accuracy of the solution for both model types. The qualitative results of the simulations are not affected by this change. The application of the ISO12-group improves the springback prediction for DX53D+Z. With this approach the position of the maximal diameter is predicted well by the models with 48 (A48I7) and 80 crystals (A80I7).

For the second material, the strain cuts are shown in Fig. 12 - 15. The values of the minor strain are slightly better with the crystal plasticity model while the results for the major strain are within the range of the reference model. The earing prediction (Fig. 16 and 17) of the crystal models is higher than the measurement.

The use of the reference models increases this overprediction. While these models predict the maximum flange draw-in at 90° with respect to the rolling direction, the crystal models predict a nearly equal flange draw-in at 0° and 90° similar to the measurements. The mean error of the crystal models is less than 1.5 mm compared with more than 2 mm in case of the reference model.

In the springback measurement, the lowest ring opens significantly for H340LAD (Fig. 18- 19). This behavior is not well predicted by the Barlat models. In fact for $m = 2$ a slight closing is predicted. The simulation with the crystal models always predicts an opening of the lowest ring. The maximum value for the ring diameter is also located at the second highest ring (2). This is well estimated by the crystal plasticity models. The Barlat 1989 model with $m = 2$ fails to predict this finding, while the model with $m = 6$ shows a dramatic decrease of the opening for the highest ring.

The increase in the number of integration points does not have any significant effect for this material. The results of the springback evaluation are given in Table 5. The usage of the ISO12-group for the isotropic background shifts the maximal diameter to the third ring resulting in a decreasing accuracy of the predicted diameter distribution.

Distance from bottom	15 mm	35 mm	55 mm	75 mm
	r in mm	r in mm	r in mm	r in mm
Meas.	79,7	93,3	95,7	93,6
B2B7	75,2	94,6	99,5	101,6
B2B9	75,5	95,8	97,2	98,2
B6B7	75,5	95,9	102,4	83,3
B6B9	75,5	90,9	100,0	103,1
B16I7	76,9	90,6	92,1	89,3
B16M7	76,7	92,6	93,1	89,3
B16M9	76,9	90,6	92,1	89,3
B32M7	76,9	93,0	93,6	90,1
B48I7	77,2	90,8	92,3	89,1
B48M7	77,0	92,2	93,5	89,3
B48M9	77,2	90,8	92,3	89,2
B64M7	77,0	93,9	94,8	92,5
B80I7	80,4	93,1	92,1	88,5
B80M7	77,1	92,6	92,9	89,2
B80M9	77,4	91,9	92,4	89,5
B96M7	77,2	92,7	93,4	89,6

Table 5: Results of the springback simulation with H340LAD
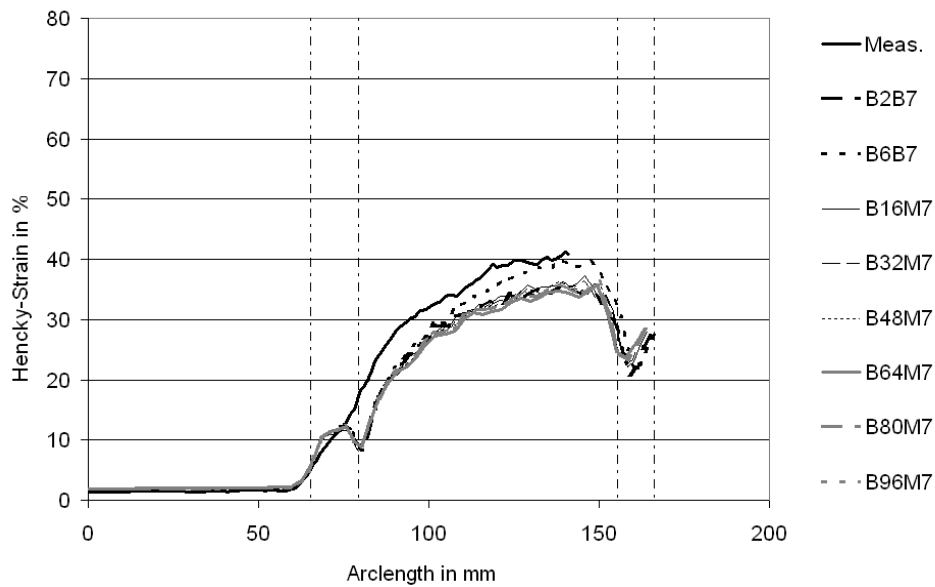
Figure 12: Major strain in rolling direction (isotropic von Mises component, H340)
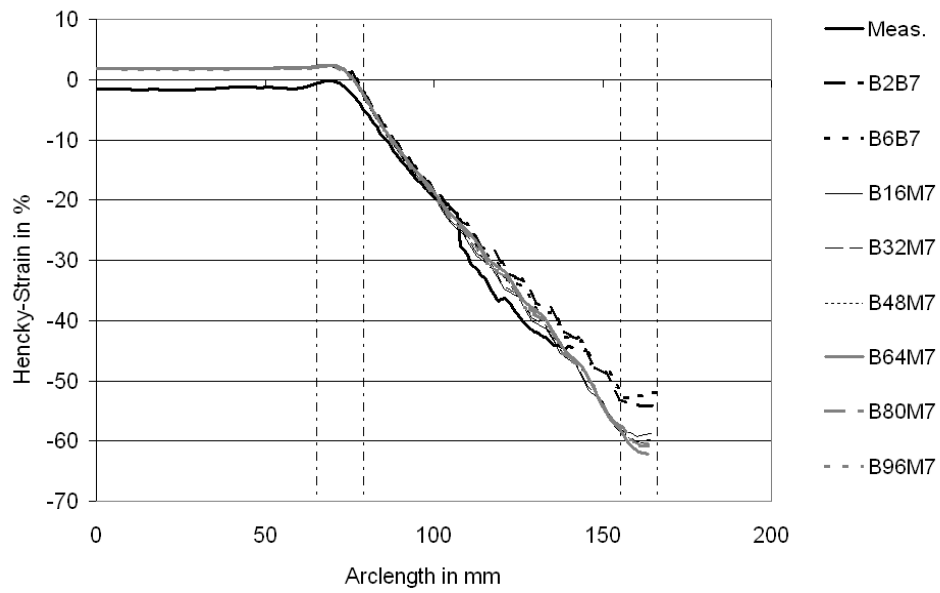
Figure 13: Minor strain in rolling direction (isotropic von Mises component, H340)
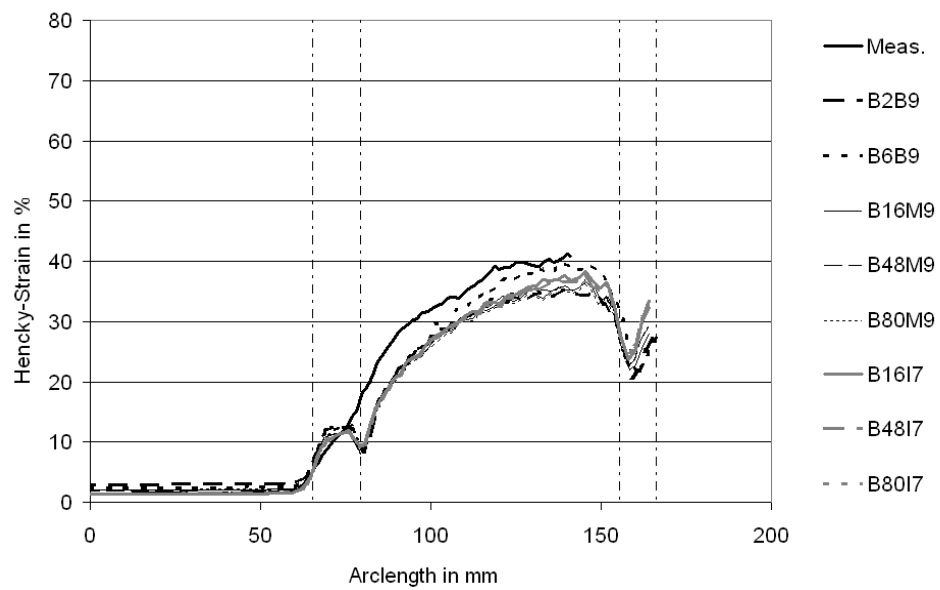

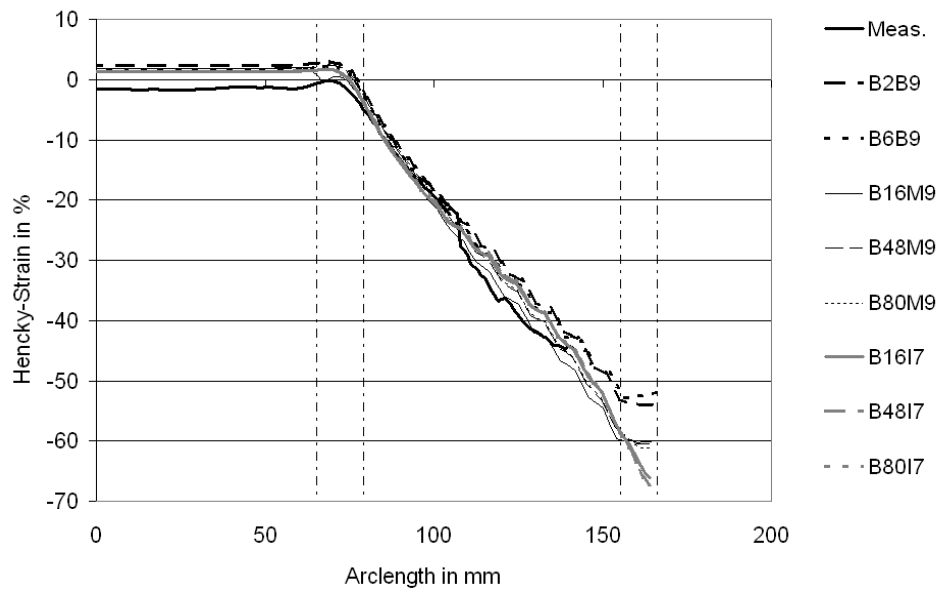Figure 14: Major strain in rolling direction (ISO12 background, H340)

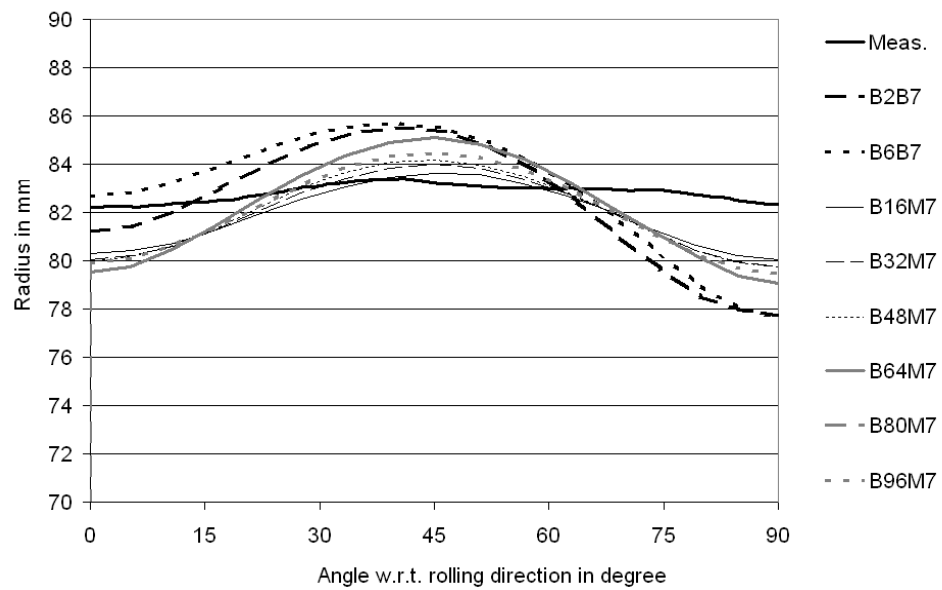Figure 15: Major strain in rolling direction (ISO12 background, H340)

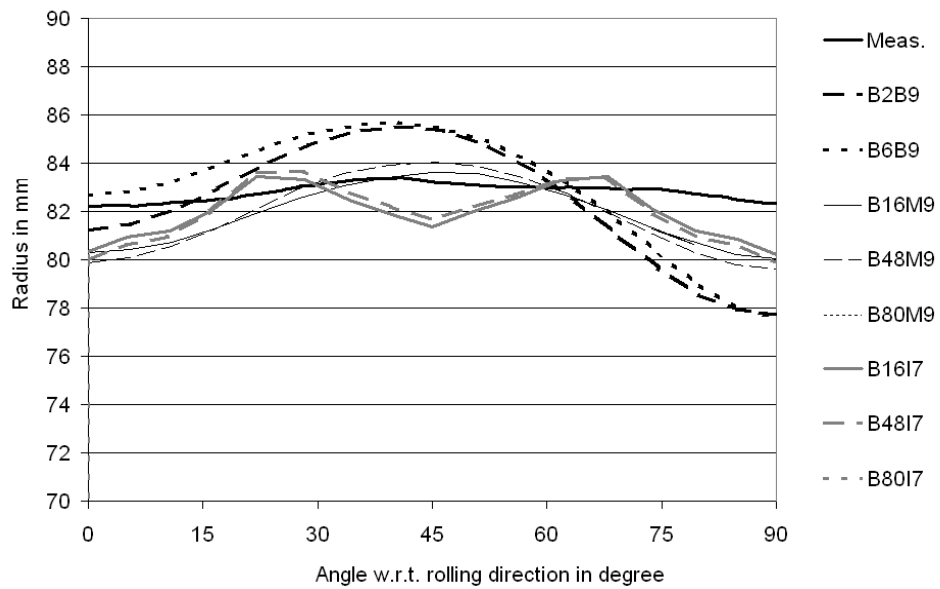Figure 16: Earing profile for models with isotropic von Mises component (H340)

152

Figure 17: Earing profile for models with ISO12 background and isotropic von Mises component (H340)
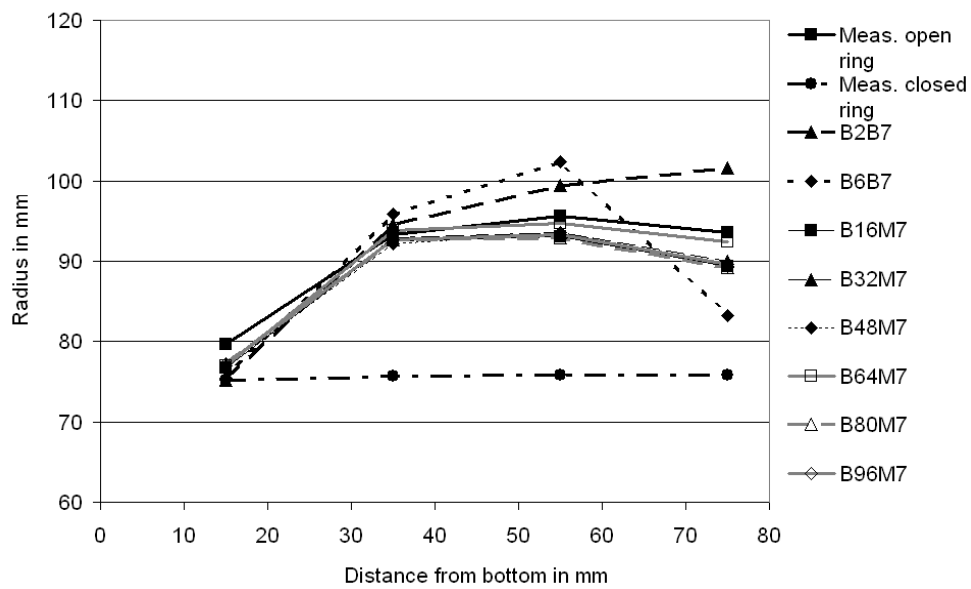

Figure 18: Springback results of H340LAD: Distribution of the ring radii: Barlat 1989 model (7 IP), crystal model with von Mises background (7 IP)
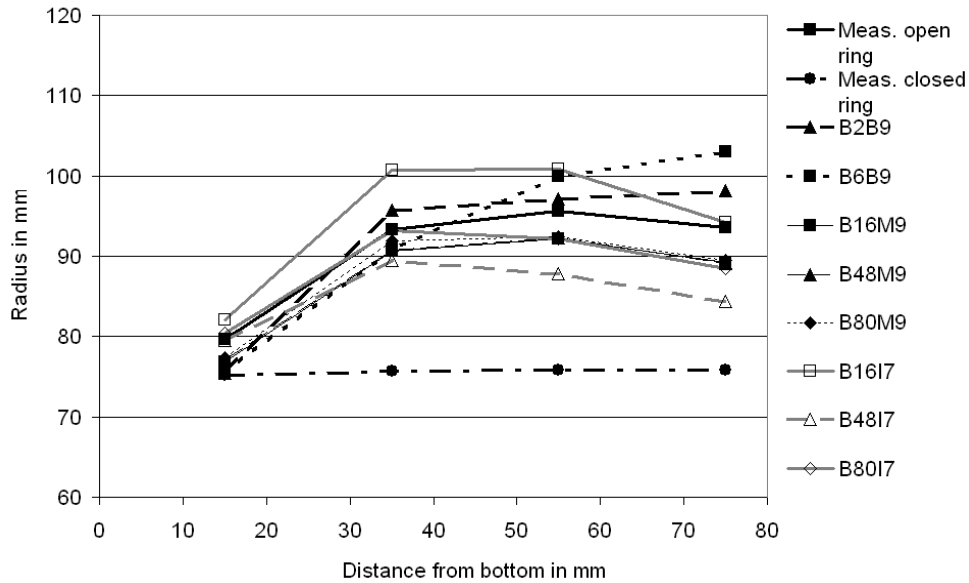
Figure 19: Springback results of H340LAD: Distribution of the ring radii: Barlat 1989 model (9 IP), crystal model with von Mises background (9 IP), crystal model with ISO12 background (7 IP)

Discussion. The evaluation of the model behavior during a deep drawing process and a subsequent cutting and springback operation shows that the number of crystals although small has only a minor influence on the simulation accuracy. The results of the strain distribution are nearly equal for all configurations under consideration. The application of the crystal plasticity model slightly improves the predictions compared to the conventional macroscopic model.

With respect to the earing, the model with the lowest number of crystals had to be rejected, since it was not able to reproduce the overall shape of the measured values. The same is true for the application of the ISO12-model for the isotropic background (gray texture) of the initial texture. The resulting earing shapes are dominated by this group, nearly independent of the other crystals. The simulation accuracy with respect to the location of the extreme values as well as the earing height is improved by using this model. The number of integration points in the thickness direction of the shell elements does not have any significant impact on the simulation accuracy with respect to the strains and the earing results. The results are within the range of other studies (Tikhovskiy et al., 2008). In this study the influence of the texture gradient is examined. In the considered materials, the texture gradient between the surface and the center are small (Schulze, 2006), so that the effort for the model setup can be reduced without a significant loss of accuracy. It also shows the influence of the different initial textures on the earing shape, similar to the study of (Raabe et al., 2005).

Considering the springback results, it can be stated that the crystal plasticity model is able to reproduce correctly the qualitative development of the springback. While the Barlat 1989 model is not able to predict the material dependent opening and closing of the lowest ring, this is achieved by the new model. The overall error of the conventional model is also higher than the one of the crystal plasticity model. Comparing the error of the springback prediction with the theoretical values that can be expected from the number of used integration points (Wagoner, 2007), we find that for the first material the maximum error is exceeding this limit, while in the second case the deviation is less than expectable. This shows that in the complex loading situation of a deep drawing process other factors (such as the friction) also have an influence on the simulation results. The increase of the number of integration points has also different results: While the result improves for the first material, it is slightly less accurate for the second. This corresponds also to the oscillation nature of the error (Wagoner, 2007).

The number of crystals does not have any significant impact on the simulation accuracy. Even with only 16 crystals, the qualitative agreement of the simulation results is good. The application of the ISO12-group seems to shift the position of the maximum diameter towards a less strained position, which increases the accuracy for material 1 and decreases it for material 2.

154

Taking all these results into consideration, the crystal plasticity model is able to improve the simulation accuracy for the given case with only 32 crystals for the approximation of the isotropic background. The option to approximate the background with the ISO12 group is less favorable since a much larger number of crystals would be needed for the background approximation, and the individual weight of these crystals would have to be of the same order as the weights for the other crystals in order not to dominate the evolution of the anisotropy.

Limitations. Due to the application of the Pencil-Glide model for the plastic deformation, different shear stresses in different glide systems, for instance due to twinning (Daniel and Jomas, 1990), cannot be simulated. Also the formation of shear bands that influence the texture evolution (Duggan et al., 1999; Leffers, 1999) and, therefore, this anisotropy is not included in this model.

The Taylor assumption that is used for the homogenization is unable to accommodate inhomogeneous deformation fields that can be observed in real materials (Boas and Hargreaves, 1948). Also the influence of the orientation of neighboring grains on the deformation mode cannot be described with this model. The textures simulated with the Taylor assumption tend to be sharper than the experimental textures and develop stable components such as the Taylor component which cannot be observed (Dawson and Beaudoin, 1998). The study by van Houtte et al. (2005) shows also the lack of this model in the course of the development of rolling textures.

The model uses a small group of crystals with volume fractions, which are not equally distributed. This can lead to an overestimation of the influence of certain crystals on the overall model behavior, as observed for instance with the ISO12-group crystal. This negative influence, however, is minor, as long as the volume fractions of the crystals have the same order of magnitude. The use of the isotropic background can also introduce problems since this part of the model remains isotropic under any deformation process. This is in contrast to the real material, in which the isotropic background consists of a large number of crystals that can develop a certain texture and therefore anisotropic material properties.

5 Conclusions

The study has shown how crystallographic information can be incorporated into a continuum mechanical modeling of sheet metal forming. Based on a specific optimization scheme, a low-dimensional description of the texture is obtained. The model is able to increase the simulation accuracy for a typical deep drawing process with a subsequent springback evaluation. The simulation results are in good agreement with the measurements, if at least 32 crystals are used. For the model identification, a texture measurement is needed in addition to the conventional tension tests in three directions of the blank. Therefore, the measurement effort is not increased dramatically. Even with such a reduced modeling, the computational effort compared with the Barlat 1989 model is increased by two orders of magnitude. Therefore, such a model will be available in the near future only with parallel computing as well as for mid size problems.

References

A. Andersson, *Numerical and experimental evaluation of springback in a front side member. J. Met. Proc. Techn.*, 169, 352–356 (2005).

M. Arminjon, Explicit relationships between texture coefficients and three-dimensional yield criteria of metals. *In: Textures of materials*, Ed: Brakman et al., Neth. Soc. Mat. Sci., 31–37 (1985).

M. Arminjon, B. Bacroix, On plastic potentials for anisotropic metals and their derivation from the texture function. *Acta Mech.*, 88, 219–243 (1990).

R.J. Asaro, A. Needleman, Overview No. 42: Texture development and strain hardening in rate-dependent polycrystals. *Acta Metall.*, 33, 923–953 (1985).

F. Barlat, D.J. Lege and J.C. Brem, A six-component yield function for anisotropic materials. *Int. J. Plast.*, 7, 693–712 (1989).

F. Barlat, J. Lian, Plastic behavior and stretchability of sheet metals. Part I: A yield function for orthotropic sheets under plane stress conditions. *Int. J. Plast.*, 5, 51-66 (1989).

F. Barlat, Y. Maeda, K. Chung, M.Yanagawa, J.C. Brem, Y. Hayashida, D.J. Lege, K. Matsui, S.J. Murtha, S. Hattori, R.C. Becker, S. Makosey, Yield function development for aluminum alloyed sheets. *J. Mech. Phys. Solids*, 11/11, 1727–1763 (1997).

F. Barlat, J.C. Brem, J.W. Yoon, K. Chung, R. E. Dick, S.H. Choi, F. Pourboghrat, E. Chu, D.J. Lege, Plane stress yield function for aluminum alloy sheets, *Int. J. Plast.*, 19, 1297–1319 (2003).

F. Barlat, H. Aretz, J.W. Yoon, M.E. Karabin, J.C. Brem, R.E. Dick, Linear transformation-based anisotropic yield functions. *Int. J. Plast.*, 21, 1009–1039 (2005).

F. Barlat, J.W. Yoon and O. Cazacu, On linear transformations of stress tensors for the description of plastic anisotropy. *Int. J. Plast.*, 23, 876-896 (2007).

R. Becker, R.E. Smelser, S. Panchanadeeswaran, Simulations of earing in aluminum single crystals and polycrystals. Modelling Simul. Mater. Sci. Eng., 1, 203–224, (1993).

A. Bertram, An alternative approach to finite plasticity based on material isomorphisms. Int. J. Plast., 15, 353–374, No. 3 (1999).

A. Bertram, T. Böhlke, N. Gaffke, B. Heiligers, R. Offinger, On the generation of discrete isotropic orientation distributions for linear elastic crystals. *J. Elast.*, 58 (2000).

A. Bertram, Elasticity and Plasticity of Large Deformations. Springer-Verlag, Berlin Heidelberg (2005).

J.F.W. Bishop, R. Hill, A theory of the plastic distorsion of polycrystalline aggregate under combined stress. Phil. Mag., 7, 42, 414–427 (1951).

J.F.W. Bishop, R. Hill, Theoretical derivation on the plastic properties of a polycrystalline face-centred metal. *Phil. Mag.*, 7, 42, 1298–1307 (1951).

W. Boas, M.E. Hargreaves, On the inhomogenity of plastic deformation in the crystals of aggregate. *Proc. Roy. Soc. London A*, 93, 89–97 (1948).

T. Böhlke, Crystallographic texture evolution and anisotropy. Simulation, modeling, and applications. Shaker (2001).

T. Böhlke, A. Bertram, Isotropic orientation distributions of cubic crystals. *J. Mech. Phys. Sol.*, 49, 2459–2470 (2001).

T. Böhlke, R. Risy, A. Bertram, Finite element simulation of metal forming operations with texture based material models. *Mod. Sim. Mat. Sci. Eng.*, 14, 365–387 (2001).

T. Böhlke, U.-U. Haus, V. Schulze, Crystallographic texture approximation by quadratic programming. *Acta Mat.*, 54, 1359–1368 (2006).

C. Bronkhorst, S. Kalidindi, L. Anand, Polycrystalline plasticity and the evolution of crystallographic texture in fcc metals. *R. Soc. Lond.* A341, 443–477 (1992).

B. Budiansky, T.T. Wu, Theoretical prediction of plastic strains of polycrystals. *Proc. 4th US Nat. Cong. Appl. Mech.*, 2, 1175 (1962).

H.J. Bunge. Texture analysis in material science. Cuvillier (1993).

H.J. Bunge, P.I. Welch, Entwicklung der Textur und der plastischen Anisotropie in Stählen durch Warmwalzen, Umwandlung und Kaltwalzen. Forschungsbericht T83-219, Bundesmin. f. Forschung und Technologie (1983).

J.-H. Cho, A.D. Rollet, K. H. Oh, Determination of volume fractions of texture components with standard distributions in Euler space. *Metall. Mat. Trans. A*, 35A, 1075–1086 (2004).

M. Crumbach, G. Pomana, P. Wagner, G. Gottstein, Recrystallisation and grain growth. In: Gottstein, G., Molodov, D. (Eds.), *Proceedings of the First Joint International Conference* (2001).

D. Daniel, J.J. Jomas, Measurement and prediction of plastic anisotropy in deep-drawing steels. *Metall. Trans. A*, 21A, 331–343 (1990).

L. Delannay, P. Van Houtte, A. Van Bael, D. Vanderschueren, Application of a texture parameter model to study planar anisotropy of rolled steel sheets. *Mod. Sim. Mat. Sci. Eng. 8*, 413–422 (2000).

P. Dawson, A. Beaudoin, K. Mathur, G. Sarma, Finite element modeling of polycrystalline solids. *Rev. europé. éléments finis*, 3, 543-571 (1994).

P.R. Dawson, A.J. Beaudoin, Finite element simulations of metal forming. In U.F. Kocks et al. *Texture and Anisotropy*, 533–558 (1998).

P.R. Dawson, S.R. MacEven, P.-D. Wu, Advances in sheet metal forming analyses: dealing with mechanical anisotropy from crystallographic texture. *Int. Mat. Rev.*, 48, 2, 86–122 (2003).

Z. Dongjuan, C. Zhenshan, R. Xueyu, L. Yuqiang, Sheet springback prediction based on non-linear combined hardening roule and Barlat89's yielding function. *Comp. Mat. Sci.*, 38, 256–262 (2006).

B.J. Duggan, E.C.H. Lim, G.L. Liu, The effects of rolling conditions and some material variables on microstructure and texture development in single phase metals and alloys. In R. K. Ray, A. K. Singh. *Textures in materials research*. 73–92, Science Publishers (1999).

O. Engler, J. Hirsch, Polycrystal-plasticity simulation of six and eight ears in deep-drawn aluminum cups. *Mat. Sci. Eng. A*, 452–453, 640–651 (2007).

J.D. Eshelby, The determination of the elastic field of an ellipsoidal inclusion and related problems. *Proc. R. Soc. London* A241, 376–396 (1957).

J.O. Hallquist, LS-DYNA theoretical manual. LSTC (1998).

S.V. Harren, R.J. Asaro, Nonuniform deformations in polycrystals and aspects of the validity of the Taylor model. *J. Mech. Phys. Solids*, 37, 191-232 (1989).

S.V. Harren, The finite deformation of rate-dependent polycrystals - I: A self-consitent framework. *J. Mech. Phys. Solids*, 39, 345–360 (1991).

S.V. Harren, The finite deformation of rate-dependent polycrystals - II: A comparison of the self-consistent and Taylor methods. *J. Mech. Phys. Solids*, 39, 361-383 (1991).

K. Helming, R.A. Schwarzer, B. Rauschenbach, S. Geier, B. Leiss, H. Wenk, K. Ullemaier, J. Heinitz, Texture estimates by means of components. *Z. Metallk.* 85, 545–553 (1994).

K. Helming, Texturapproximation durch Modellkomponenten. Cuvillier Verlag Göttingen (1996).

R. Hill, A theory of the yielding and plastic flow of anisotropic metals. *Proc. Royal Soc. London A*, 193, 281–297 (1948).

R. Hill, Continuum micro-mechanics of elastoplastic polycrystals. *J. Mech. Phys. Sol.*, 13, 89–101 (1965).

H. Honneff, H. Mecking, A method for the determination of the active slip systems and orientation changes during single crystal deformation. *ICOTOM 5*, 1, 265–275 (1978).

J. Hu, J.J. Jonas, T. Ishikawa, FEM simulation of the forming of textured aluminum sheets. *Mat. Sci. Eng. A*, 256, 51–59 (1998).

S.R. Kalidindi, L. Anand, An approximate procedure for predicting the evolution of crystallogrphic textures in bulk deformation processing of fcc metals. *Int. J. Mech. Sci.*, 34, 3099–3129 (1992).

U.F. Kocks, G.R. Canova, How many slip systems, and which?. N. Hansen, Deformation of polycrystals - mechanisms and microstructure. *Proc. 2nd RisøSymp.*, 35–44 (1981).

U. Kocks, J. Kallend, A. Biondo, Accurate representation of general textures by a set of weighted grains. *Text. Microstruct.* 14-18, 199–204, ICOTOM 9, Special Issue (1991).

U. F. Kocks, C. T. Necker, Polycrystal models to fit experiments. *15th RisøInt. Symp. Mat. Sci.* (1994).

A. Krawietz, Materialtheorie. Springer-Verlag (1986).

A. Krawietz, Parallel versus conventional elastoplasticity. *Technische Mechanik*, 19, 279–288, No. 4 (1999).

E. Kröner, Zur plastischen Verformung des Vielkristalls. *Acta Metall.*,9, 155–161 (1961).

M. Kuroda and V. Tvergaard,Effects of texture on shear band formation in plane strain tension/compression and bending. *Int. J. Plasticity*, 23, 244–272 (2007).

E.H. Lee, Elastic-plastic deformation at finite strains. *J. Appl. Mech.*, 36, 1–6 (1969).

T. Leffers, Microstructure - the forgotten factor in texture models. In R. K. Ray, A. K. Singh. Textures in materials research. 93–110, Science Publishers (1999).

S. Li, E. Hoferlin, A. Van Bael, P. Van Houtte, C. Teodosiu, Finite element modeling of plastic anisotropy induced by texture and strain-path change. *Int. J. Plast.*, 19, 647–674 (2003).

A. Makinouchi, Elastic-Plastic Stress Analysis of U-Bend Processes of Sheet Metal. *Adv. Techn. Plast.*, 1, 672–677 (1985).

J. Mandel, Thermodynamics and plasticity. Proc. Int. Symp. Foundations of Continuum Thermodynamics, McMillan, London. Edts. Delgado Domingos, J.J. and Nina, M.N. and Whitlaw, J.H., 283 (1974).

K. Mathur and P.R. Dawson, On modeling the development of crystallographic texture in bulk forming processes. *Int. J. Plast.*, 5, 67–94 (1989).

K. Mattiasson, A. Strange, P. Thiderkvist, A. Samuelsson, Simulation of Springback in Sheet Metal Forming. *Proc. 5th Int. Conf. Num. Meth. Ind. Form. Proc.*, 115–124, (1995).

P.J. Maudlin, S.I. Wright, U.F. Kocks, M.S. Sahota, An application of multisurface plasticity theory: yield surfaces of textured materials, *Acta Mat.*, 44, 4027–4032 (1996).

A. Molinari, G. Canova, S. Ahzi, A self consistent approach of the large deformation polycrystal viscoplasticity. Acta Metall. 35, 2983 (1987).

F. Montheillet, P. Gilormini, J.J. Jonas, Relation between axial stresses and texture development during torsion testing: a simplified theory. *Acta Metall.*, 33, 705–717 (1985).

C. Miehe, J. Schotte, Anisotropic finite elastoplastic analysis of shells: simulation of earing in deep-drawing of single- and polycrystalline sheets by Taylor-type micro-to-macro transition. *Comp. Meth. Appl. Mech. Eng.*, 193, 25–57 (2004).

R. von Mises. Mechanik fester Körper im plastisch-deformablen Zustand. Nachrichten von der Gesellschaft der Wissenschaften zu Göttingen, Mathematisch-Physikalische Klasse, 582-592 (1913).

D. Raabe, M. Sachtleber, Z. Zhao, F. Roters, S. Zaefferer, Micromechanical and macromechanical effects in grain scale polycrystal plasticity experimentation and simulation. *Acta Mat.*, 49, 3433–3441 (2001).

D. Raabe, P. Klose, B. Engl, K.-P. Imlau, F. Friedel, F. Roters, Concepts for integrating plastic anisotropy into metal forming simulations. Advanced Engineering Materials, 4(4), 169–180 (2002).

D. Raabe, F. Roters, Using texture components in crystal plasticity finite element simulations. *Int. J. Plast.*, 20, 339–361 (2004).

D. Raabe, Y. Wang, F. Roters, Crystal plasticity simulation study of the inluence of texture on earing in steel. *Comp. Mat. Sci.*, 34, 221–234 (2005).

M. Rohleder, Simulation rückfederungsbedingter Formabweichungen im Produktentstehungsprozeß von Blechformteilen. Shaker (2002).

G. Sachs, H. Schumann, K. Czrener, W. Molle, H. Oettel, J. Ohser, H.-L. Steyer, Zur Ableitung einer Fließbedingung. Z. Verein dt. Ing., 72, 734–736 (1928).

V. Schulze, Anwendung eines kristallplastischen Materialmodells in der Umformsimulation. PhD Thesis, Universität Magdeburg (2006).

H. Schumann, K. Czrener, W. Molle, H. Oettel, J. Ohser, H.-L. Steyer, Metallographie. Dt. Verl. F. Grundstoffindustrie (1991).

J. Tarasiuk, K. Wierzbanowski, B. Bacroix, Texture decomposition into gauss-shaped functions: classical and genetic algorithm methods. *Comp. Mat. Sci.* 29, 179–186 (2004).

G.I. Taylor, Plastic strain in metals. *J. Inst. Metals*, 62, 307–324 (1938).

I. Tikhovskiy, D. Raabe, F. Roters, Simulation of earing of 17% stainless steel considering texture gradients. *Mat. Sci. Eng.* A, (2008), doi:10.1016/j.msea.2007.11.063

L. Toth, P. Van Houtte, Discretization techniques for orientation distribution functions. *Text. Microstruct.* 19, 229–244 (1992).

C.N. Tomé, G.R. Canova, U.F. Kocks, N. Christodoulou, J.J. Jonas, The relation between macroscopic and microscopic strain hardening in f.c.c. polycrystals. *Acta Metall.*, 32, 1637–1653 (1984).

F. Valente, D. Traversa, Springback Calculation of Sheet Metal Parts after Trimming and Flanging. Proc. 4th Int. Conf. Works. *Num. Sim. 3-D Sheet Metal Forming*, 59–64 (1999).

P. Van Houtte, Adaptation of the Taylor theory to the typical substructure of some cold rolled fcc metals. ICOTOM 6, 428–433 (1981).

P. Van Houtte, On the equivalence of the relaxed taylor theory and the bishop-hill theory for partially constrained plastic deformation of crystals. *Materials Science and Engineering* 55, 69–77 (1982).

P. Van Houtte, Assessment of macroscopic strain heterogenities in relaxed constraints models for the prediction of deformation textures. *ICOTOM 8*, 349 (1988).

P. Van Houtte, L. Delannay, S. Kalidini, Comparison of two grain interaction models for polycrystal plasticity and deformation texture prediction. *Int. J. Plast.* 18, 359–377 (2002).

P. Van Houtte, S. Li, M. Seefeldt, L. Dellanay. Deformation texture prediction: from the Taylor model to the advanced Lamel model. *Int. J. Plast.*, 21, 589–624 (2005).

P. Van Houtte, A. Kanjarla, A. Van Bael, M. Seefeldt, L. Delannay, Multiscale modelling of the plastic anisotropy and deformation texture of polycrystalline materials. *Europ. J. Mech. A/Solids* 25, 634–648 (2006).

R.H. Wagoner, N. He, Springback Simulation in Sheet Metal Forming. *NUMISHEET 3*, 308–315 (1996).

R.H. Wagoner, Simulation of springback: Through-thickness integration. *Int. J. Plast.* 23, 345–360 (2007).

G. Wassermann. Texturen metallischer Werkstoffe. Springer (1939).

P.I. Welch, Techniques for the determination of complete pole figures using composite specimens. *Texture of Crystalline Solids* 4, 99 (1980).

P.D. Wu, D.J. Lloyd, M. Jain, K.W. Neale and Y. Huang, Effects of spatial grain orientation distribution and initial surface topography on sheet metal necking. *Int. J. Plasticity* 23 (2007).

W.L. Xu, C.H. Ma, C.H. Li, W.J. Feng, Sensitive factors in springback simulation for sheet metal forming. *J. Mat. Proc. Tech.*, 151, 217–222 (2004).

J.W. Yoon, S.H. Hong, Modeling of aluminum alloy sheets based on new anisotropic yield functions. *J. Mat. Proc. Tech.*, 177, 134–137 (2006).

F. Yoshida, T. Uemori, A model of large-strain cyclic plasticity and its application to springback simulation. *Int. J. Mech. Sci.*, 45, 1687–1702 (2993).

Addresses:

Dr.-Ing. V. Schulze, Volkswagen AG, EKAB Funktionsauslegung Ausstattung und Methoden, Postfach 1697/4, Germany, email: `volker.schulze@volkswagen.de`

Prof. Dr.-Ing. A. Bertram, Otto-von-Guericke-Universität Magdeburg, Institut für Mechanik, Postfach 4120, 39016 Magdeburg, Germany, email: `bertram@mb.uni-magdeburg.de`

Prof. Dr.-Ing. T. Böhlke, Universität Karlsruhe (TH), Institut für Technische Mechanik, Postfach 6980, 76128 Karlsruhe, Germany, email: `boehlke@itm.uni-karlsruhe.de`

Prof. Dr.-Ing. A. Krawietz, Technische Fachhochschule Berlin, Fachbereich VIII, Luxemburger Str.10, 13353 Berlin, Germany, email: `krawietz@t-online.de`